

See discussions, stats, and author profiles for this publication at: <https://www.researchgate.net/publication/49736387>

Elemental Imaging via Laser Ionization Orthogonal Time-of-Flight Mass Spectrometry

ARTICLE in ANALYTICAL CHEMISTRY · FEBRUARY 2011

Impact Factor: 5.64 · DOI: 10.1021/ac1029693 · Source: PubMed

CITATIONS

8

READS

43

6 AUTHORS, INCLUDING:



Rongfu Huang

University of Alberta

26 PUBLICATIONS 186 CITATIONS

[SEE PROFILE](#)



Wei Hang

Shanghai University of Finance and Economics

102 PUBLICATIONS 1,318 CITATIONS

[SEE PROFILE](#)



Jian He

Xiamen University

31 PUBLICATIONS 238 CITATIONS

[SEE PROFILE](#)



Benli Huang

Xiamen University

93 PUBLICATIONS 1,202 CITATIONS

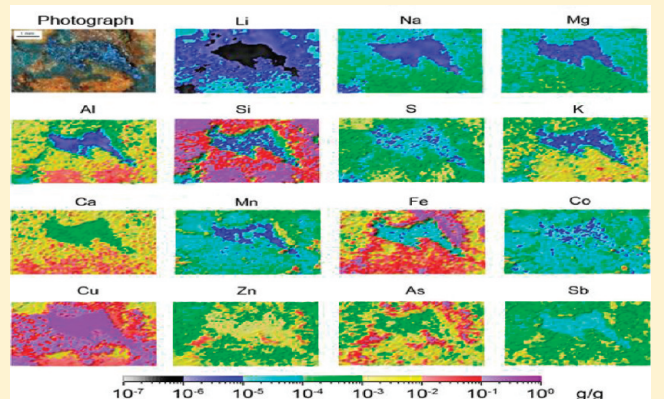
[SEE PROFILE](#)

Elemental Imaging via Laser Ionization Orthogonal Time-of-Flight Mass Spectrometry

Rongfu Huang,[†] Bochao Zhang,[†] Dongxuan Zou,[†] Wei Hang,^{*,†,‡} Jian He,[§] and Benli Huang[†]

[†]Key Laboratory of Analytical Sciences, College of Chemistry and Chemical Engineering, [‡]State Key Laboratory of Marine Environmental Science, and [§]Department of Mechanical and Electrical Engineering, Xiamen University, Xiamen 361005, China

ABSTRACT: An elemental imaging method using a laser ionization orthogonal time-of-flight mass spectrometer system was developed for the simultaneous detection of all metal and nonmetal elements. The instrument control and data processing were realized by self-developed programs. This system is capable of simultaneous detection of metal and nonmetal elements, with a spatial resolution of $50\text{ }\mu\text{m}$, the lowest detection limits of $3 \times 10^{-7}\text{ g/g}$ (Li), and a dynamic range of 7 orders of magnitude. Moreover, this technique does not require standards for quantitative analysis and can be a powerful and versatile tool for elemental imaging.



Imaging mass spectrometry has received great interest in recent years and has been used to analyze various kinds of biological and geological solids, providing information on the distribution of elements and molecules.^{1–6} Laser ablation inductively coupled plasma mass spectrometry (LA-ICPMS) and secondary ion mass spectrometry (SIMS) are commonly applied for elemental imaging of solid surfaces.^{5–9} Limitations still exist for these elemental imaging techniques, such as the inability to identify some nonmetallic elements, matrix effects, elemental fractionation, and the requirement of standards for quantitation.^{1,5,6,8–11} Meanwhile, a sample required for imaging analysis normally comprises materials with different matrixes, and it is extremely difficult to find a series of imaging standards containing different matrixes for quantitative calibration.

A high-irradiance laser ionization orthogonal time-of-flight mass spectrometry (LI-O-TOFMS) system is capable of direct solid analysis as well as standardless semiquantitation.^{12–14} Unlike traditional laser ionization mass spectrometry, LI-O-TOFMS uses a buffer-gas-assisted ion source and an orthogonal TOF geometry.¹⁵ With our instrument setup, the matrix effect is reduced significantly under the conditions of high laser irradiance and inert buffer gas.¹⁶ High laser irradiance ($\geq 10^{10}\text{ W/cm}^2$) generates a plasma with a temperature as high as $\sim 50\text{ 000 K}$, which greatly minimizes the elemental fractionation associated with the element properties (e.g., melting and boiling points and ionization potentials). Inert gas in the source can cool ions with a large kinetic energy distribution to improve the resolving power of the system and also expedite the charge reduction via three-body recombination, which diminishes the interference of multiply charged ions to a negligible level.¹⁸ Orthogonal TOF-MS decouples the ion transmission

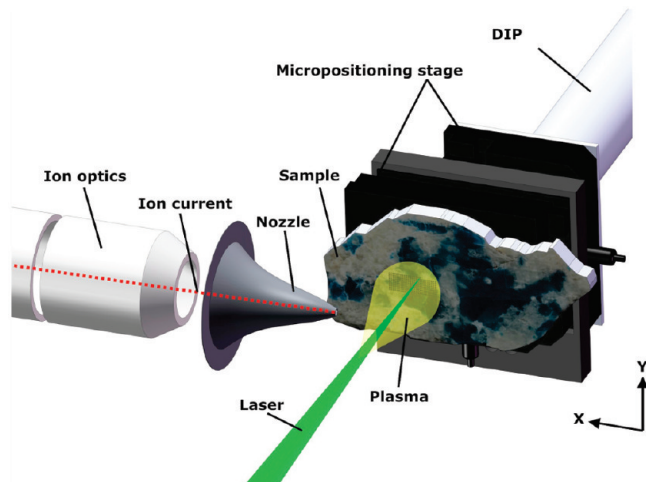


Figure 1. Schematic diagram of the ion source in the LI-O-TOFMS system.

direction and the TOF direction, which further enhances the resolving power. Because of these features, LI-O-TOFMS has a dynamic range of 7 orders of magnitude and close relative sensitivity coefficients for different elements,¹³ which paves the way for simultaneous metal and nonmetal elemental imaging and standardless quantitation.

Received: November 11, 2010

Accepted: December 17, 2010

Published: January 7, 2011

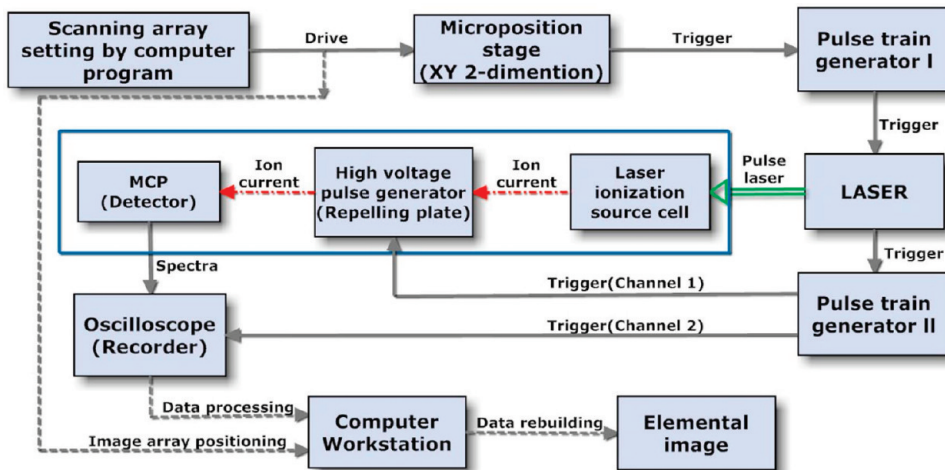


Figure 2. Measurement procedure of the elemental imaging LI-O-TOFMS system.

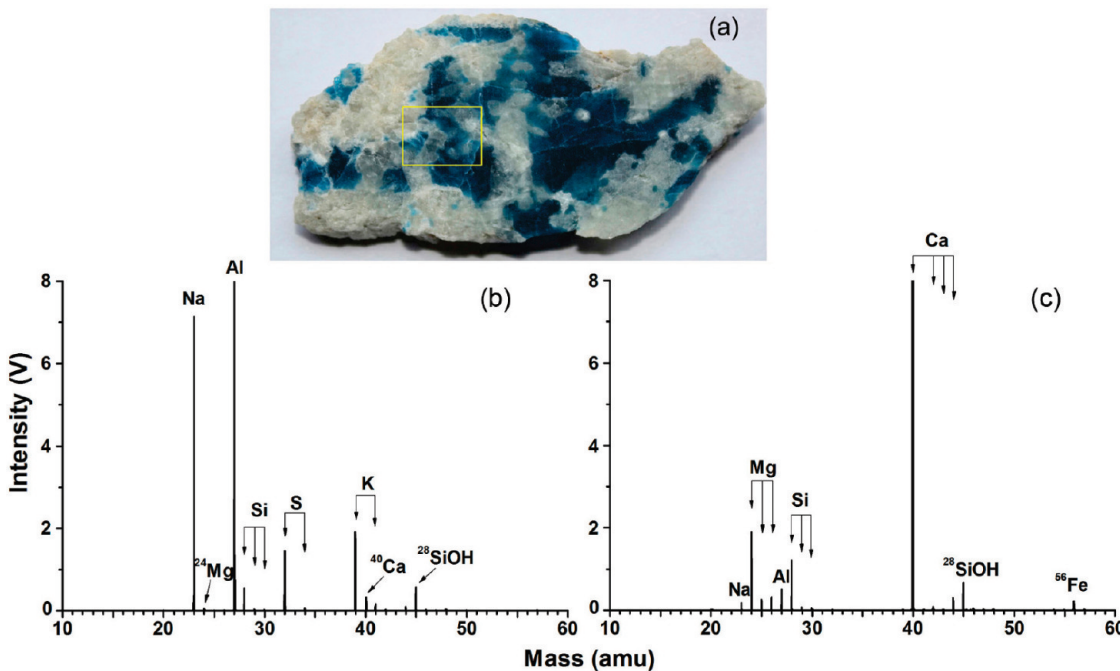


Figure 3. (a) Photograph of the aluminum mineral sample. The imaging area, marked by yellow lines, was scanned using an array of 120×85 spots at $50 \mu\text{m}$ spot intervals. Typical mass spectra are shown for (b) the blue and (c) the white areas.

EXPERIMENTAL SECTION

All the experiments were carried out on an in-house-built laser ionization orthogonal time-of-flight mass spectrometer system that has been described previously with only a few modifications.^{12–14,19} Mass spectrometry parameters were optimized previously,^{12,13} and appropriate parameters were adopted in this experiment. As shown in Figure 1, the laser had a wavelength of 532 nm, a pulse length of 4.4 ns, a frequency of 10 Hz, and an irradiance of $4 \times 10^{10} \text{ W/cm}^2$. Low-pressure helium ($\sim 700 \text{ Pa}$) was utilized in the source for both collisional cooling of the energetic ions and charge reduction of multiply charged ions. An XY two-stage micropositioner (Physik Instrumente) was used for sample positioning; the precision of the micropositioner was in the micrometer range. The general scanning array for imaging

was 120×85 spots with $50 \mu\text{m}$ intervals. The total acquisition time required for imaging a normal array (125×85 spots) was about 11 h due to the fixed laser frequency of 10 Hz in this experiment. An aluminum mineral sample and a copper mineral sample were analyzed in this experiment. Each sample surface was polished to prevent physical spikes before the sample was mounted in the source.

The entire measurement procedure is illustrated in Figure 2. The control system was driven by a computer program that defined the parameters of the laser scanning array. Multifunction cards (National Instruments) were used as pulse train generator I and pulse train generator II and controlled by self-developed LabVIEW programs. The laser was used on the external control mode and controlled by pulse train generator I that generates

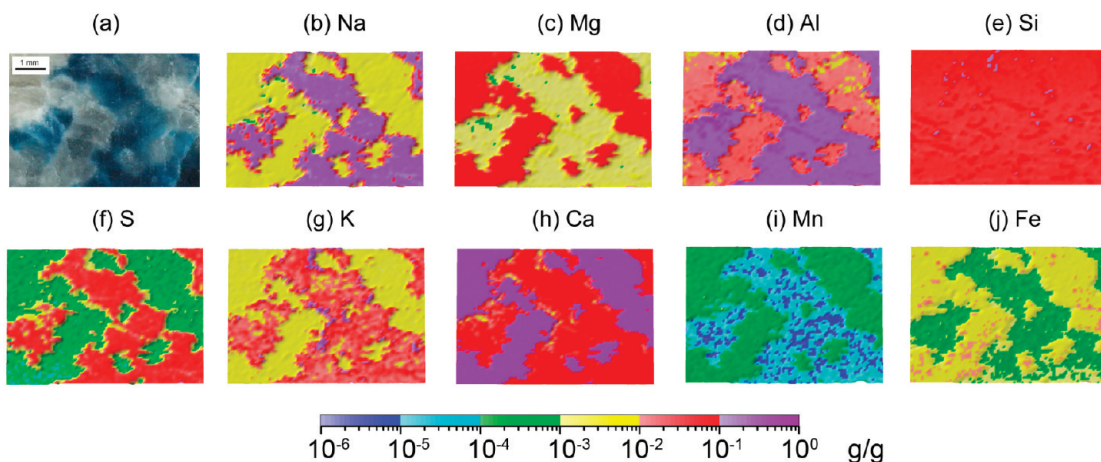


Figure 4. (a) Photograph of the imaging area of the aluminum mineral sample and the elemental images for (b) Na, (c) Mg, (d) Al, (e) Si, (f) S, (g) K, (h) Ca, (i) Mn, and (j) Fe.

pulse trains to trigger the laser, thus hitting each array spot on the surface with a fixed pulse number. Pulse train generator II was used as the dual-channel sync output, which simultaneously triggered the high-voltage pulse generator for the repelling pulse and the oscilloscope recorder. Data, originating from both the oscilloscope recorder and the scanning array setting program, were processed to construct elemental images using a self-developed LabVIEW program. The final image was presented using Surfer software.

RESULTS AND DISCUSSION

An aluminum mineral sample was initially investigated using LI-O-TOFMS. This sample was mainly comprised of two different compositions as shown by blue and white areas in Figure 3a. Typical mass spectra of the differently colored areas are shown in Figure 3b,c. Elements contained in the aluminum mineral sample, such as Na, Mg, Al, S, K, Ca, Mn, and Fe, were distributed differently between the blue and white areas. Both spectra (Figure 3b,c) are explicit with no significant interference, except for that from SiOH^+ , which is the result of the high oxide bonding energy of silicon (800 kJ/mol) and was considered in the calculation of the silicon concentration.¹⁸

The laser spot diameter of approximately 50 μm represents the image resolution for the experiment. The laser beam can be focused to an area less than 10 μm across after the laser beam passes through the focus objective; however, the spot is heated to expand to 50 μm after 40 ablation pulses. A lower pulse number for a single spot can result in a higher image resolution but will reduce the sensitivity as fewer spectra are accumulated. In our experiment, 40 pulses per spot were required to reach an LOD of $\mu\text{g/g}$ with an image resolution of 50 μm .

A photograph of the exact imaging area and the distributions of the elements are presented in Figure 4. It is clear that Na, S, and Al were found primarily in the blue area, while Ca, Mg, Mn, and Fe were located mainly in the white area, and the amount of Si was not significantly different between the two areas. The images of Na and S match well, suggesting the presence of Na_2S or Na_2SO_4 . This Na-containing compound was identified as Na_2S because a subsequent digestion experiment revealed that the blue material was reductive in reaction with HNO_3 . Further investigation indicated that the blue color resulted from aluminum oxide and the white color was derived from calcium and

Table 1. Comparison of the Elemental Concentrations (g/g) in the Aluminum Mineral Determined by ICPMS after Digestion and Directly by LI-O-TOFMS

| element | blue part | | white part | |
|-----------------|-------------------|-------------------|-------------------|-------------------|
| | ICPMS | LI-O-TOFMS | ICPMS | LI-O-TOFMS |
| Na | 1.4×10^5 | 1.7×10^5 | 2.6×10^3 | 4.0×10^3 |
| Mg | 1.2×10^3 | 1.6×10^3 | 7.0×10^4 | 8.3×10^4 |
| Al | 1.4×10^5 | 1.8×10^5 | 6.4×10^3 | 1.2×10^4 |
| Si ^a | | 4.0×10^4 | | 4.5×10^4 |
| S ^a | | 3.9×10^4 | | 5.6×10^2 |
| K | 4.3×10^3 | 1.2×10^4 | 2.6×10^3 | 3.2×10^3 |
| Ca | 4.7×10^4 | 7.7×10^4 | 2.3×10^5 | 3.0×10^5 |
| Mn | 1.9×10^1 | 2.2×10^1 | 5.2×10^2 | 5.5×10^2 |
| Fe | 6.0×10^2 | 5.1×10^2 | 7.7×10^3 | 8.5×10^3 |

^a Quantitation was not available by ICPMS.

magnesium carbonates. The concentrations of the elements plotted in Figure 4 were determined according to the standardless semiquantitation method.¹³

For inert-gas-assisted high-laser-irradiance-source mass spectrometry, the spectra contain little interference (as shown in Figure 3b,c); matrix effects and elemental fractionation are small, and the relative sensitivities for most elements are close to unity.¹⁶ Thus, the ratio of an individual elemental signal to the summed signal from all elements should be approximately the molar composition of that element, because the signal intensity is directly proportional to the number of ions reaching the detector. This method can be used for the semiquantitation analysis without standards for calibration. The elemental concentration is calculated as follows:

$$w_j = \sum_i A_{ij} M_{ij} / \sum_j \sum_i A_{ij} M_{ij} \quad (1)$$

where A_{ij} represents the peak intensity of isotope i of element j , M_{ij} represents the molar mass of isotope i of element j , and w_j represents the mass fraction (element concentration) of element j . For geological samples that are abundant in oxygen, the second M_{ij} in eq 1 is usually replaced by the molar mass of its typical oxide state (e.g., MgCO_3 , Al_2O_3 , SiO_2 , K_2O , CaCO_3 , MnO_3 , and

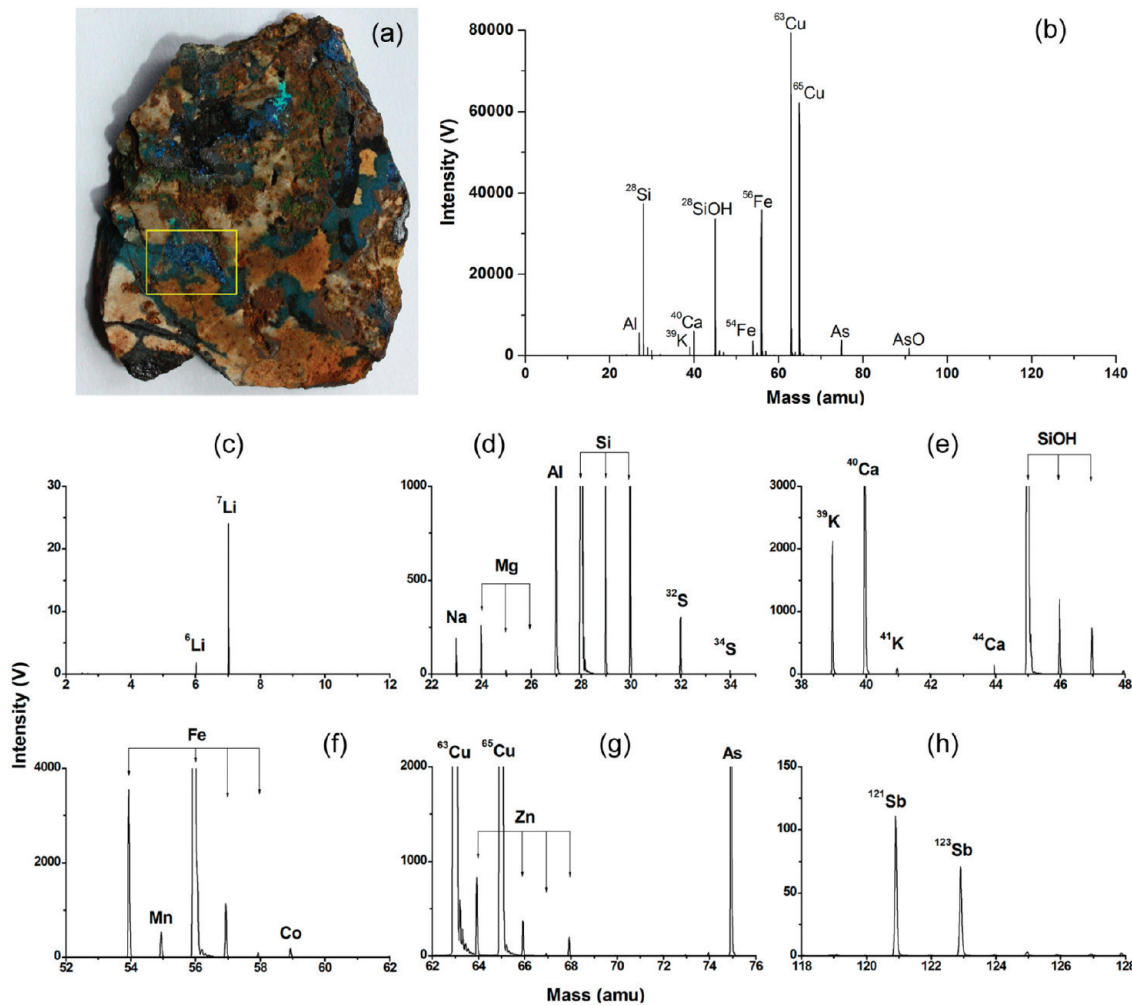


Figure 5. (a) Photograph of a copper mineral sample. The imaging area is marked by yellow lines. (b) Accumulated spectrum of the entire imaging area. Magnified portions of the spectrum at (c) 2–12, (d) 22–35, (e) 38–48, (f) 52–62, (g) 62–76, and (h) 118–128 amu.

Fe_2O_3 for elements Mg, Al, Si, K, Ca, Mn, and Fe, respectively). This replacement is done because oxygen cannot be ionized effectively under normal operation conditions due to its high ionization potential,²⁰ but it must be considered in the element quantitation.

We concluded that this sample was bauxite on the basis of its elemental composition.²¹ For comparison, elemental concentrations were measured by ICPMS (Agilent) after separated digestions of blue and white materials, and the results are listed in Table 1. The results from ICPMS and LI-O-TOFMS are in good agreement. Slightly higher concentrations are observed using LI-O-TOFMS, which might be caused by the omission of the species in the calculation, such as oxygen (from both the sample and the residue in the buffer gas) and water (from vapor in the buffer gas and crystalline water in the mineral).

A copper mineral sample (shown in Figure 5a) was further investigated using the LI-O-TOFMS imaging system. The entire spectral accumulation method was used, which allows the clear identification of all trace elements, even on tiny areas, and the further verification of the minor isotope peaks of these elements in a single spectrum. It can also reflect the overall elemental compositions for inhomogeneous samples. The mass spectrum of the entire imaging area is shown in Figure 5b, which is magnified in Figure 5c–h. Li, Na, Mg, Al, Si, S, K, Ca, Mn, Fe, Co, Cu, Zn,

As, and Sb were detected. The polyatomic ions SiOH^+ and AsO^+ were also observed and counted as partial intensities for Si and As.

A photograph of the imaging area is shown in Figure 6a, and all of the element images are shown in Figure 6b–p. A blue area was present in the center of the imaging area, surrounded by the brown area (Figure 6a). Copper was detected abundantly in the blue area, and zinc was also concentrated in the blue area, although its concentration was 2 orders of magnitude lower than that of copper. Iron and silicon were distributed mainly in the brown area. All other trace elements were located primarily in the surrounding brown area, including the nonmetal elements Si, S, and As. The elemental distributions are illustrated in Figure 6, with concentration information provided. The lowest detectable concentration (3×10^{-7} g/g) was found for Li in the center area of the image (see the black area in Figure 6b and the spectrum in Figure 5c).

CONCLUSION

Imaging mass spectrometric techniques using LI-O-TOFMS were developed for investigating the distribution of elements in mineral samples. LI-O-TOFMS is capable of simultaneous, sensitive, and semiquantitative imaging of metals and nonmetals

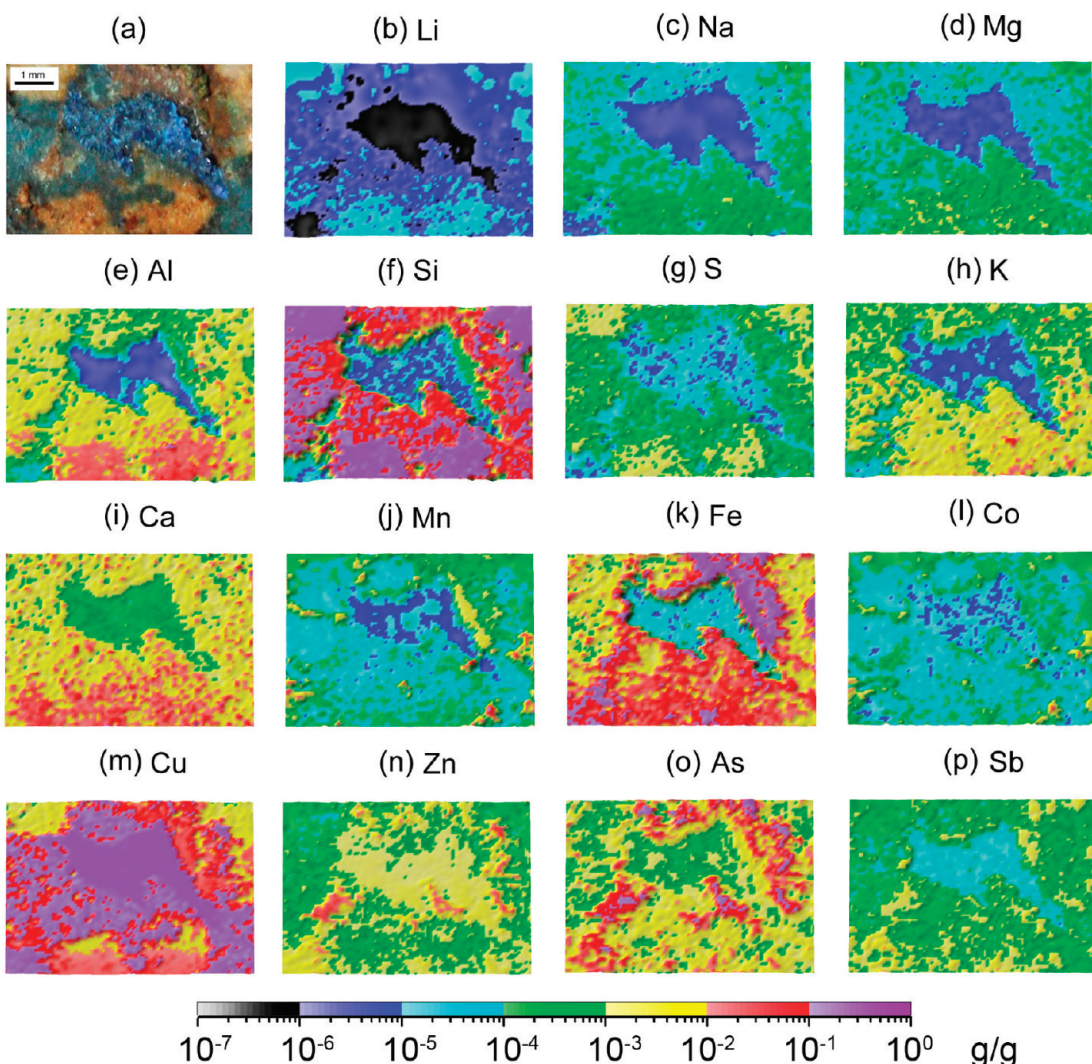


Figure 6. (a) Photograph of the imaging area on the surface of a copper mineral sample. Elemental images of (b) Li, (c) Na, (d) Mg, (e) Al, (f) Si, (g) S, (h) K, (i) Ca, (j) Mn, (k) Fe, (l) Co, (m) Cu, (n) Zn, (o) As, and (p) Sb.

for solids. The system reached detection limits of 10^{-7} g/g and a dynamic range of 7 orders of magnitude. More importantly, it does not require standards for semiquantitative analysis. All these features give this technique the potential to be a powerful and convenient tool in elemental imaging of solid surfaces. If equipped with an ultrashort pulsed laser which minimizes the thermal effect and matrix effect, the system should provide even higher lateral resolution and more precise standardless quantitative results.

■ ACKNOWLEDGMENT

Financial support from the Natural Science Foundation of China (Grants 20775063 and 21027011) and the National 863 program (Grant 2009AA06Z109) is gratefully acknowledged. This work has also been supported by NFFTBS (Grant J1030415).

■ REFERENCES

- (1) Becker, J. S.; Zoriy, M.; Matusch, A.; Wu, B.; Salber, D.; Palm, C.; Becker, J. S. *Mass Spectrom. Rev.* **2010**, *29*, 156–175.
- (2) Eberlin, L. S.; Ifa, D. R.; Wu, C.; Cooks, R. G. *Angew. Chem., Int. Ed.* **2010**, *49* (873–876), S873/1–S873/11.
- (3) Pacholski, M. L.; Winograd, N. *Chem. Rev.* **1999**, *99*, 2977–3005.
- (4) Seeley, E. H.; Caprioli, R. M. *Proteomics—Clin. Appl.* **2008**, *2*, 1435–1443.
- (5) Wu, B.; Zoriy, M.; Chen, Y.; Becker, J. S. *Talanta* **2009**, *78*, 132–137.
- (6) Large, R. R.; Danyushevsky, L.; Hollit, C.; Maslennikov, V.; Meffre, S.; Gilbert, S.; Bull, S.; Scott, R.; Emsbo, P.; Thomas, H.; Singh, B.; Foster, J. *Econ. Geol.* **2009**, *104*, 635–668.
- (7) Ulrich, T.; Kamber, B. S.; Jugo, P. J.; Tinkham, D. K. *Can. Mineral.* **2009**, *47*, 1001–1012.
- (8) Becker, J. S.; Zoriy, M.; Dressler, V. L.; Wu, B.; Becker, J. S. *Pure Appl. Chem.* **2008**, *80*, 2643–2655.
- (9) Boxer, S. G.; Kraft, M. L.; Weber, P. K. *Annu. Rev. Biophys.* **2009**, *38*, 53–74.
- (10) Carmona, A.; Cloetens, P.; Deves, G.; Bohic, S.; Ortega, R. *J. Anal. At. Spectrom.* **2008**, *23*, 1083–1088.
- (11) Zoriy, M. V.; Dehnhardt, M.; Matusch, A.; Becker, J. S. *Spectrochim. Acta, Part B* **2008**, *63*, 375–382.
- (12) Li, L.; Zhang, B.; Huang, R.; Hang, W.; He, J.; Huang, B. *Anal. Chem.* **2010**, *82*, 1949–1953.
- (13) Yu, Q.; Huang, R.; Li, L.; Lin, L.; Hang, W.; He, J.; Huang, B. *Anal. Chem.* **2009**, *81*, 4343–4348.
- (14) Yu, Q.; Chen, L.; Huang, R.; Hang, W.; He, J.; Huang, B. *Trends Anal. Chem.* **2009**, *28*, 1174–1185.

- (15) He, J.; Huang, R.; Yu, Q.; Lin, Y.; Hang, W.; Huang, B. *J. Mass Spectrom.* **2009**, *44*, 780–785.
- (16) Yu, Q.; Li, L.; Zhu, E.; Hang, W.; He, J.; Huang, B. *J. Anal. At. Spectrom.* **2010**, *25*, 1155–1158.
- (17) Vertes, A., Gijbels, R., Adams, F., Eds. *Laser Ionization Mass Analysis*; Wiley Interscience: New York, 1993.
- (18) Huang, R.; Yu, Q.; Tong, Q.; Hang, W.; He, J.; Huang, B. *Spectrochim. Acta, Part B* **2009**, *64*, 255–261.
- (19) Tong, Q.; Yu, Q.; Jin, X.; He, J.; Hang, W.; Huang, B. *J. Anal. At. Spectrom.* **2009**, *24*, 228–231.
- (20) Lide, D. R., Ed. *Handbook of Chemistry and Physics*, 84th ed.; CRC: Boca Raton, FL, 2004.
- (21) Kusky, T. *Encyclopedia of Earth Science*. Facts On File: New York, 2005.